

Beyond maps: Patterns of formation processes at the Middle Pleistocene open-air site of Marathousa 1, Megalopolis Basin, Greece

D. Giusti^{a,*}, V. Tourloukis^a, G. E. Konidaris^a, N. Thompson^b, P. Karkanas^c,
E. Panagopoulou^d, K. Harvati^a

^a*Paläoanthropologie, Senckenberg Centre for Human Evolution and Palaeoenvironment, Eberhard Karls Universität Tübingen, Rümelinstr. 23, 72070 Tübingen, Germany*

^b*Friedrich-Alexander University of Erlangen-Nürnberg, Institute of Prehistory and Early History, Kochstr. 4/18, 90154 Erlangen, Germany*

^c*Malcolm H. Wiener Laboratory for Archaeological Science, American School of Classical Studies at Athens, Greece*

^d*Ephoreia of Palaeoanthropology-Speleology of Greece, Athens, Greece*

Abstract

Recent excavations at the Middle Pleistocene open-air site of Marathousa 1 have unearthed in one of the two investigated area (Area A) a partial skeleton of a single individual of *Elephas (Palaeoloxodon) antiquus* and other faunal remains in spatial and stratigraphic association with lithic artefacts. In Area B, a much higher number of lithic artefacts was collected, spatially and stratigraphically associated with other faunal remains. The two areas are stratigraphically correlated, the main fossiliferous layers representing an *en masse* depositional process in a lake margin context. Evidence of butchering (cut-marks) has been identified on two bones of the elephant skeleton, as well on other mammal bones from Area B. However, due to the secondary deposition nature of the main find-bearing units, it is of primary importance to evaluate the degree and reliability of the spatial association of the lithic artefacts with the faunal remains. Indeed, spatial association does not necessarily imply causation. The present study uses a comprehensive set of multiscale and multivariate spatial statistics, in order to disentangle the depositional processes behind the distribution of the archaeological and palaeontological record at Marathousa 1. Moving beyond distribution maps,

*Corresponding author

Email address: domenico.giusti@uni-tuebingen.de (D. Giusti)

statistical inference allows for a better interpretation of spatial patterns by adopting a more inductive and reproducible strategy. Moreover, within a frame of references, it enables us to depict the underlying processes responsible for the observed patterns, and to quantify the extent of the post-depositional reworking processes which have long been recognised to affect the integrity of archaeological assemblages. Assessing the degree of disturbance is crucial to fully comprehend the archaeological record, and therefore to reliably interpret past human behaviours. Preliminary results of our analyses suggest minor reworking and substantial spatial association of the lithic and faunal assemblages, supporting the current interpretation of Marathousa 1 as a butchering site.

Keywords: Spatial taphonomy, Vertical distribution, Fabric analysis, Point pattern analysis, Site formation processes, Middle Pleistocene

1. Introduction

The analysis of archaeological site formation and modification processes, intensively studied since the early 1970s (Isaac, 1967; Schiffer, 1972, 1983, 1987; Shackley, 1978; Wood and Johnson, 1978; Schick, 1984, 1986, 1987; Petraglia and Nash, 1987; Petraglia and Potts, 1994, among others), is nowadays fully integrated in the archaeological practice. Drawing inferences about past human behaviours from scatters of archaeological remains must account for depositional and post-depositional contextual processes.

Several methods are currently applied in order to qualify and quantify the type and degree of reworking of archaeological assemblages. Within the framework of a geoarchaeological and taphonomic approach, spatial statistics offer meaningful contributions in unravelling site formation and modification processes from spatial patterns.

The study of the clast fabric (dip and strike of elongated sedimentary particles, including bones and artefacts), first addressed by Isaac (1967); Bar-Yosef and Tchernov (1972); Schick (1986), has more recently been found to successfully discriminate between sedimentary processes (Bertran and Texier, 1995; Bertran et al., 1997), leading to a noteworthy development of methods and propagation of applications in Palaeolithic site formation studies (Lenoble and Bertran, 2004; Lenoble et al., 2008; McPherron,

19 2005; Benito-Calvo et al., 2009; Benito-Calvo and de la Torre, 2011; Benito-Calvo
20 et al., 2011; Bernatchez, 2010; Domínguez-Rodrigo et al., 2012; García-Moreno et al.,
21 2016; Sánchez-Romero et al., 2016, among others).

22 The vertical distribution of materials, on the other hand, has been long investigated
23 with the aim of identifying cultural levels, by visually interpreting virtual profiles (but
24 see Anderson and Burke (2008) for a quantitative approach).

25 However, archaeological horizons may be subject to vertical rearrangement by syn-
26 and post-depositional processes. Several experimental studies have investigated the
27 effect of trampling on the vertical displacement of artefacts (Villa and Courtin, 1983;
28 Gifford-Gonzalez et al., 1985; Nielsen, 1991; Eren et al., 2010). Although these works
29 have reported a negative correlation between artefact size and vertical displacement,
30 particle size sorting of lithic assemblages, when exposed to physical geomorphic agents
31 (such as gravity, water flow, waves and tides, wind), has been widely documented
32 (Rick, 1976; Schick, 1986; Petraglia and Nash, 1987; Morton, 2004; Lenoble, 2005;
33 Bertran et al., 2012).

34 Bone and lithic refitting analysis is an additional, particularly robust method in
35 investigating the stratigraphic integrity of a site (Villa, 1982, 1990; Todd and Stanford,
36 1992; Morin et al., 2005; Sisk and Shea, 2008). Furthermore, lithic refits have been
37 shown to provide reliable clues about the spatio-temporal dimension of past human
38 behaviours, by discriminating activity areas (López-Ortega et al., 2011, 2015; Vaquero
39 et al., 2012, 2015; Clark, 2016).

40 Finally, distribution maps are cornerstones of the archaeological documentation
41 process and are primary analytic tools. However, their visual interpretation is prone
42 to subjectivity and is not reproducible. Since the early 1970's (see Hodder and Or-
43 ton (1976); Orton (1982) and references therein), the traditional, intuitive, 'eyeballing'
44 method of spotting spatial patterns has been abandoned in favour of more objective ap-
45 proaches, extensively borrowed from other fields. Nevertheless, quantitative methods,
46 while still percolating in the archaeological sciences from neighbouring disciplines, are
47 not extensively used. Moreover, only a relatively small number of studies have explic-
48 itly applied spatial point pattern analysis or geostatistics to the study of site formation
49 and modification processes (Lenoble et al., 2008; Domínguez-Rodrigo et al., 2014b,a,

50 2017; Carrer, 2015; Giusti and Arzarello, 2016; Organista et al., 2017, but see Hivernel
51 and Hodder (1984) for an earlier work on the subject).

52 The goal of a taphonomic approach to spatial analysis is to move beyond distribution
53 maps by applying a comprehensive set of multiscale and multivariate spatial statistics,
54 in order to reliably infer processes from spatial patterns. An exhaustive spatial analytic
55 approach to archaeological inference, combined with a taphonomic perspective,
56 is essential for the evaluation of the integrity of the archaeological assemblage, and
57 consequently for a reliable interpretation of past human behaviours.

58 **2. Marathousa 1**

59 The object of the present study is the spatial distribution of the archaeological and
60 palaeontological record recovered during excavation at the Middle Pleistocene open-air
61 site of Marathousa 1, Megalopolis, Greece (Panagopoulou et al., 2015; Harvati et al.,
62 2016).

63 The site (Fig. 1), discovered in 2013 at the edge of an active lignite quarry, is located
64 between lignite seams II and III in the Pleistocene deposit of the Megalopolis basin,
65 Marathousa Member of the Choremi Formation (van Vugt et al., 2000). The regular
66 alternation of lacustrine clay, silt and sand beds with lignite seams has been interpreted
67 having cyclic glacial (or stadial) and interglacial (or interstadial) origin (Nickel et al.,
68 1996). The half-graben configuration of the basin, with major subsidence along the
69 NE-SW trending normal faults at the eastern margin, resulted in the gentle dip of the
70 lake bottom at the opposite, western, margin of the lake, enabling the formation of
71 swamps and the accumulation of organic material for prolonged periods of time (van
72 Vugt et al., 2000).

73 Two excavation areas have been investigated since 2013: Area A, where several
74 skeletal elements of a single individual of *Elephas (Palaeoloxodon) antiquus* have been
75 unearthed, together with a number of lithic artefacts (Konidaris et al., this volume;
76 Tourloukis et al., this volume); and Area B, about 60 m to the South along the exposed
77 section, where the lithic assemblage is richer and occurs in association with a faunal as-
78 semblage composed by isolated elephant bones, cervids and carnivores among others.

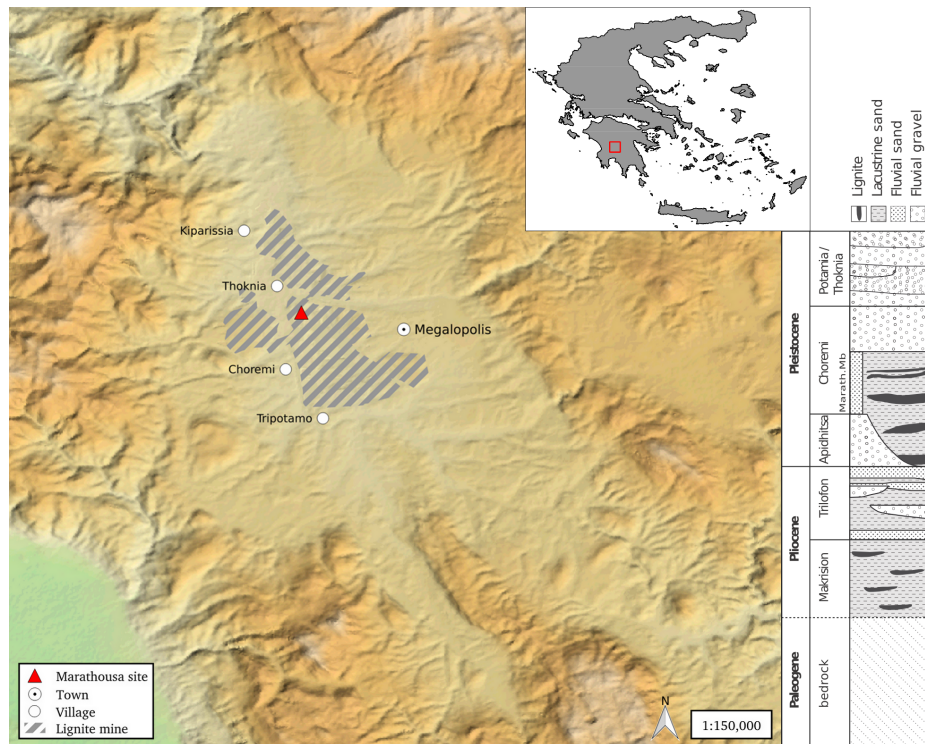


Figure 1: Geographical location of the Marathousa 1 site in the Megalopolis basin and stratigraphic column, modified after [van Vugt et al. \(2000\)](#).

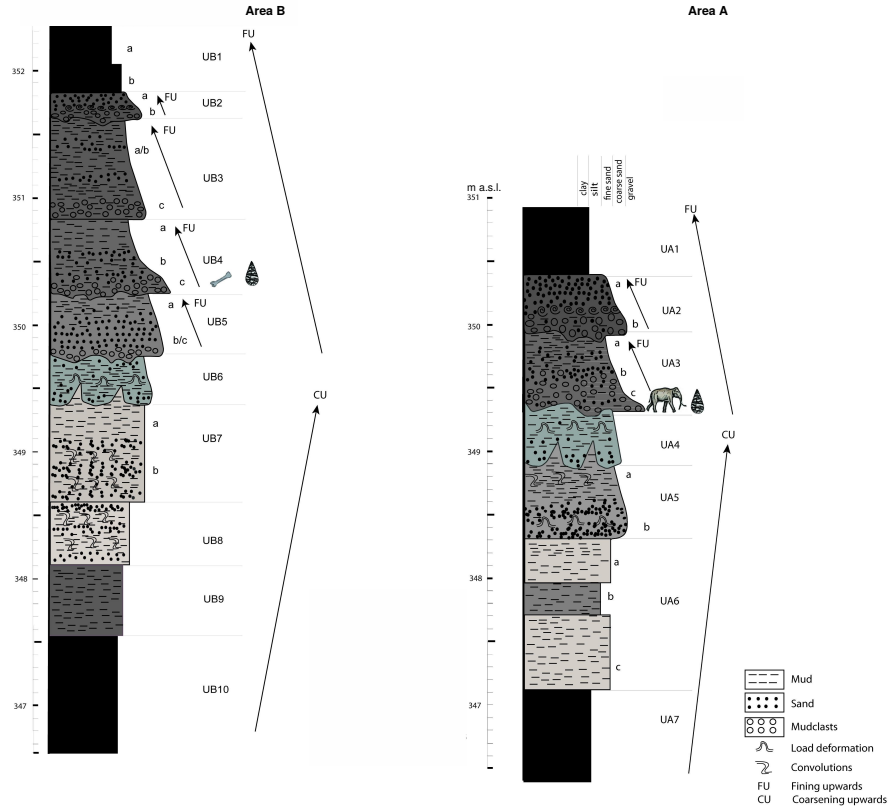


Figure 2: Stratigraphic setting of the Marathousa 1 site, modified after Karkanas et al. (this volume).

79 Evidence of butchering (cut-marks) have been identified on two of the elephant bones
 80 from Area A, as well on elephant and other mammal bones from Area B (Konidaris et
 81 al., this volume).

82 An erosional contact separates the two main find-bearing units in both areas, namely
 83 UA3c/4 and UB4c/5a (Fig. 2). In Area A, the elephant remains lie at the contact of
 84 UA3c/4 and are covered by UA3c. In Area B, most of the material were collected from
 85 unit UB4c. For both areas, the working hypothesis is that the flow event represented by
 86 units UA3c and UB4c eroded an exposed surface (where the elephant was lying) and
 87 scoured this surface, thereby entraining clastic material (including probably artefacts)
 88 and re-depositing it at close distance (see Karkanas et al., this volume).

89 The erosional event described above, and specifically the erosional contacts be-
90 tween the fossiliferous horizons in the two areas, provide the essential background for
91 the analysis and interpretation of the spatial distributions at Marathousa 1.

92 The secondary deposition nature of the main find horizons raises the question of
93 how reliable is the spatial association between the lithic artefacts and the partial skele-
94 ton of a single individual of *Elephas (Palaeoloxodon) antiquus* and the other faunal
95 remains. Since spatial association does not necessarily imply causation, the answer has
96 important consequences for the interpretation of the site in the broader context of the
97 Middle Pleistocene human-proboscidean interactions. We aim to tackle this question
98 and disentangle the formation processes acting at Marathousa 1 on the basis of spatial
99 patterns through a three-prong spatial analytic approach:

- 100 1. by analysing, in a frame of references, the fabric of remains from relevant strati-
101 graphic units;
- 102 2. by quantifying and comparing their relative vertical distributions;
- 103 3. by identifying spatial trends in either the assemblage intensities and the associa-
104 tions between classes of remains.

105 **3. Material and methods**

106 Since 2013, systematic investigation of the Marathousa 1 site has been carried out
107 by a joint team from the Ephoreia of Palaeoanthropology-Speleology (Greek Ministry
108 of Culture) and the University of Tübingen. A grid of 1 square meter units was set up,
109 oriented -14 degrees off the magnetic North, and including the two areas of investiga-
110 tion. The excavation of the deposit proceeded into sub-squares of 50x50 cm in Area
111 B and 1x1 m squares in Area A, and spits of about 5 to 10 cm thickness, respectively.
112 Systematic screen-washing of sediments was carried out on-site using 1 mm sieves,
113 in order to guarantee recovery of the small-size fraction (e.g., micro-artefacts, small
114 mammal remains, fish, molluscs and small fragments of organic and inorganic mate-
115 rial). The three-dimensional coordinates of finds (i.e., all the lithic artefacts, teeth and
116 diagnostic bones; bones and organic material with a-axis \geq 20 mm), collected spits
117 of sediment, samples and geological features (e.g., erosional contacts and mud cracks)

118 were recorded with the use of a Total Station. The dimensions (length, width and thick-
119 ness) of registered finds were measured on-site with millimetre rules. Orientation (dip
120 and strike) of elongated particles (i.e., faunal remains, large wood fragments and lithic
121 artefacts) was recorded since 2013 with a 30 degree accuracy, using a clock-like sys-
122 tem (the strike was measured, relatively to the grid North, in twelve clockwise slices).
123 In 2015, the use of a compass and inclinometer with an accuracy of 1 degrees was in-
124 troduced in Area B to gradually replaced the former method. Strike (azimuth) and dip
125 measurements were taken along the a-axis (symmetrical longitudinal axis) of the bones
126 ([Domínguez-Rodrigo and García-Pérez, 2013](#)), the lithic artefacts ([Bertran and Texier,](#)
127 [1995](#)) and organic material, using the lowest endpoint of the axis as an indicator of the
128 vector direction.

129 The present study focuses on the excavated stratigraphic units in which most of the
130 archaeological and palaeontological remains were recovered in both excavation areas,
131 namely UA3c and UA4 in Area A, and UB4c and UB5a in Area B. From the total,
132 subset samples of material were used for each specific spatial analysis. For the fabric
133 analysis we included material collected until 2016. For the vertical distribution and
134 point pattern analyses, the region of investigation was limited to the squares excavated
135 from 2013 until 2015, 25 and 29 square meters respectively in each area.

136 The analyses were performed in R statistical software ([R Core Team, 2016](#)). In
137 order to make this research reproducible ([Marwick, 2017](#)), a repository containing
138 a compendium of data, source code and text is open licensed available at the DOI:
139 [10.5281/zenodo.822273](https://doi.org/10.5281/zenodo.822273)

140 *3.1. Fabric analysis*

141 Comparative fabric analysis was conducted with the aim to investigate the dynam-
142 ics of the depositional processes at Marathousa 1. The analysis of the orientation of
143 elongated clasts can distinguish three main types of pattern (isotropic, planar and linear
144 fabric), each one associated with different sedimentary processes.

145 At the margin of a lacustrine environment, relatively close to the surrounding relief,
146 a combination of high- and low-energy processes can be expected. According to the
147 depositional context of the site (Karkanas et al., this volume), a strong preferred ori-

148 entation of clasts (linear pattern) would suggest the action of massive slope processes
149 such as mudslides and debris / hyperconcentrated flows. On the other hand, whereas
150 the frontal lobes of debris flows have been found to show a more random orientation
151 (isotropic pattern), overland flows have been associated with planar fabrics ([Lenoble](#)
152 and [Bertran, 2004](#)). Conversely, in a lacustrine floodplain, anisotropy without signif-
153 icant transport can be caused by low-energy processes such as lake transgression and
154 regression, as well as water-sheet formed during rainy seasons. Isotropic patterns have
155 been observed in different parts of mudflats as well ([Cobo-Sánchez et al., 2014](#)).

156 Nevertheless, grey zones exist between different depositional processes, so that an
157 unequivocal discrimination based only on fabric observations is often not possible, and
158 other taphonomic criteria must also be considered.

159 Since fabric strength has been found to be positively correlated with the shape
160 and size of the clast, for the fabric analysis we subset samples of remains with length
161 ≥ 2 cm and elongation index (the ratio length/width) $I_e \geq 1.6$ ([Lenoble and Bertran,](#)
162 [2004](#)). The samples are listed in Table 1 and include mostly wood fragments and
163 faunal remains from the four stratigraphic units studied here. No distinction of skeletal
164 elements was made, both due to the high fragmentation rate of faunal remains in Area
165 B, and because recent experiments showed a similar orientation pattern for different
166 bone shapes ([Domínguez-Rodrigo and García-Pérez, 2013; Domínguez-Rodrigo et al.,](#)
167 [2012](#)).

168 The sample of bones belonging to the individual of *Elephas (P.) antiquus* from
169 Area A was analysed separately and included the humerus, ulna, femur and tibia; the
170 atlas, axis and 16 complete vertebrae or vertebra fragments; 29 complete ribs or rib
171 fragments; 2 calcanea; 4 metatarsals/metacarpals; the pyramidal; the trapezoid and the
172 pelvis. The sample from UB5a was too small (only 7 observations) and was therefore
173 excluded. The sample from the UB4c unit was divided in two sub-samples consid-
174 ered separately: those recorded using the clock method and those recorded using the
175 compass method. All the sampled observations are representative of the whole area of
176 interest.

177 Rose diagrams and uniformity tests, such as Rayleigh, Kuiper, Watson and Rao
178 tests ([Jammalamadaka et al., 2001](#)), were used to visualise and evaluate circular isotropy

Table 1: List of sampled observations for the fabric analysis.

Sample	<i>n</i>	Type		
		Fauna	Wood	Lithic
UA3c	49	23	25	1
UA4	38	8	30	-
<i>E. (P.) antiquus</i>	63			
UB4c (clock)	86	68	4	14
UB4c (compass)	65	47	10	8

in the sample distribution. The Rayleigh test is used to assess the significance of the sample mean resultant length (\bar{R}), assuming that the distribution is unimodal and not bi- or plurimodal. The \bar{R} ranges from 0 to 1: values close to 1 indicate that the data are closely clustered around the mean direction; when the data are evenly spread \bar{R} has a value close to 0. A *p-value* lower than 0.05 rejects the hypothesis of randomness with a 95% confidence interval. Kuiper, Watson and Rao are omnibus tests used to detect multimodal departures from circular uniformity. All of them were applied using a significance level of *alpha* = 0.01. The test results were evaluated against critical values: a result higher than the critical value rejects the null hypothesis of isotropy with a 99% confidence interval.

Randomness testing of three-dimensional data was conducted with the Woodcock S_1/S_3 test (Woodcock and Naylor, 1983). Considering both the dip (plunge) and strike (bearing) of the oriented items, this method, based on three ordered eigenvalues (S_1 , S_2 , S_3), is able to discriminate the shape and strength of the distributions. The shape parameter $K = \frac{\ln(S_1/S_2)}{\ln(S_2/S_3)}$ ranges from zero (uni-axial girdles) to infinite (uni-axial clusters). The parameter $C = \ln(S_1/S_3)$ expresses the strength of the preferential orientation, and its significance is evaluated against critical values from simulated random samples of different sizes. A perfect random uniform distribution would have $C = 0$ and $K = 1$.

The Benn (Benn, 1994) diagram adds to the Woodcock test an isotropy ($IS = S_3/S_1$) and an elongation ($ES = 1 - (S_2/S_1)$) index. Like the former method, it is able to differentiate between linear (cluster), planar (girdle) or isotropic distributions.

201 There are no published raw data from actualistic studies on depositional processes af-
202 fecting the orientation of bones and artefacts deposited on lacustrine floodplains (but
203 see [Morton \(2004\)](#) and [Cobo-Sánchez et al. \(2014\)](#) as pioneer studies on this subject).
204 However, we included in the Benn diagram references to published results from obser-
205 vation of fabrics in modern subaereal slope deposits ([Bertran et al., 1997](#); [Lenoble and](#)
206 [Bertran, 2004](#)).

207 Fabric analysis is a powerful tool but, as suggested by [Lenoble and Bertran \(2004\)](#),
208 it is not sufficient to unequivocally discriminate processes and should therefore be in-
209 tegrated with the analysis of other diagnostic features.

210 *3.2. Vertical distribution*

211 We provisionally assume that a general concentration of unsorted material in the
212 proximity of the erosional surfaces would support an autochthonous origin of the as-
213 semblages; whereas a poorly to extremely poorly sorted and homogeneous vertical dis-
214 tribution of remains from the UA3c and UB4c units would suggest an allochthonous
215 origin and a subsequent secondary deposition triggered by a massive process, e.g., de-
216 bris or hyperconcentrated flows. Graded bedding could result in such fluid depositional
217 environments, associated with a decrease in transport energy.

218 In order to estimate the degree of vertical dispersion while controlling for the size
219 of the archaeological material, dimensional classes were set up following typological
220 criteria. Lithic artefacts were classified as debris/chip when smaller than a cutoff length
221 of 15 mm (see Tourloukis et al., this volume). Other classes include flakes, tools and
222 cores; the latter being the bigger and heavier debitage product. Table 2 summarises
223 the sample size for each class. Lithic debris/chips constitutes the larger part of the
224 assemblages from UB4c (60%) and UB5a (49%); whereas in Area A it represents only
225 a moderate percentage in the upper UA3c unit (16%). The very rare presence of lithic
226 artefacts in the underlying unit UA4 is nevertheless significant. In this unit, the faunal
227 remains are also found in much lower numbers, their number reduced to one fourth
228 of those found in UA3c. For the point pattern analysis (see below), we used the same
229 subset of materials for both excavation areas.

Table 2: List of sampled observations for the vertical distribution and point pattern analyses.

Sample	<i>n</i>	Lithic class					Faunal class			
		Debris/chip	Flake	Bone flake	Tool	Core	Indet.	Bone	Tooth	Microfauna
UA3c	279	46	2	-	1	-	1	171	14	44
UA4	61	3	1	-	-	-	-	45	4	8
UB4c	1243	753	154	1	34	6	2	246	28	19
UB5a	101	50	12	-	3	-	-	30	3	3

230 For Area B, the material recovered from the water-screening was randomly provenanced according to the 5 cm depth of the excavated spit and the coordinates of the 231 50x50 cm quadrant of the excavation square. Following the same excavation protocol, 232 the same procedure was applied for the water-screened material of Area A, which was 233 randomly provenanced according to 3D-coordinates of the 1x1 m excavation square 234 and 10 cm spit.

235 Inverse-distance weighting (IDW) interpolation of the recorded points of contact 236 between the UB4c/5a and UA3c/4 stratigraphic units were used to reconstruct their 237 erosional surfaces, in Areas A and B, respectively (Fig. 3a,b). IDW assumes spatial 238 autocorrelation and calculates, from a set of irregular known points, weighted average 239 values of unknown points. Thus, in order to address our specific objective, i.e., to 240 quantify and analyse the vertical distribution of the archaeological and palaeontological 241 material, we measured the minimum orthogonal distance of each specimen to the 242 interpolated erosional surface (Fig. 3c).

243 For the units above and below this surface (i.e., UB4c and UB5a), the relative 244 distribution of lithic classes and faunal remains was informally tested by means of 245 kernel density estimations. Likewise, in Area A the relative vertical distribution of 246 remains from UA3c was estimated relative to the absolute elevation of the elephant 247 remains and the range of elevations of the UA3c/4 surface. Finally, a Student's two 248 sample t-test allowed us to compare the empirical distributions of different groups of 249 remains for each stratigraphic unit.

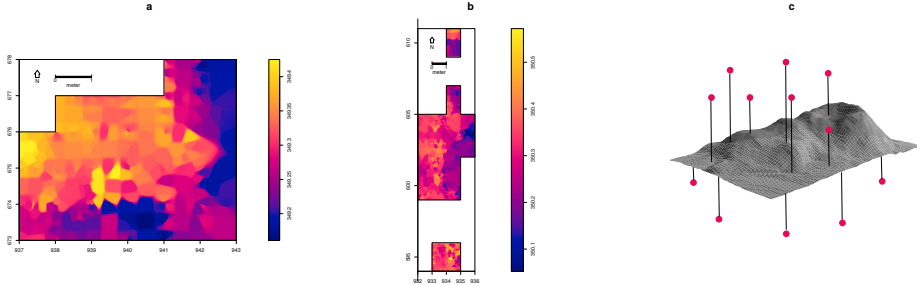


Figure 3: IDW interpolation of the UA3c/4 (a) and UB4c/5a (b) points of erosional contact; the color scale denotes elevation a.s.l. Illustration of the method used to quantify the vertical dispersion of remains with respect to the UB4c/5a surface (c).

251 3.3. *Point pattern analysis*

252 A spatial point pattern is defined as the outcome of a random spatial point process
 253 (repetitions of it would always create a different pattern). The observed patterns of the
 254 archaeological and palaeontological remains were treated as manifestations of spatial
 255 point processes, i.e., site formation processes. Point pattern analysis investigates the
 256 spatial arrangement of points with the aim to identify spatial trends. In order to inte-
 257 grate the previous studies of the fabric and vertical distributions, we directed our point
 258 pattern analysis equally to the intensity of the patterns (the rate of occurrence of the
 259 recorded finds) and to the spatial interaction between different types of finds.

260 As the average number of random points per unit area, intensity informs about ho-
 261 mogeneity or inhomogeneity in the distribution of events generated by a point process,
 262 i.e., whether the rate of occurrence is uniform or spatially varying across the study area.
 263 Intensity, usually non-parametrically evaluated by means of kernel density estimation
 264 (Diggle, 1985), was assessed for the distribution of material from the UB4c, UB5a
 265 and UA3c units. Cross-validation bandwidth, which assumes a Cox process, and edge
 266 correction were applied using the methods described in Diggle (1985).

267 In the presence of a covariate, it is recommended to further investigate the depen-
 268 dence of intensity on that explanatory variable. In order to evaluate whether variation
 269 in the density of materials was correlated to the topography of the erosional surface,
 270 we computed a local likelihood smoothing estimate of the intensity of remains from

271 UB4c as a function of the UB4c/5a surface elevation model (Baddeley et al., 2012).
272 Formal tests enabled us to assess the evidence of that dependence and to quantify the
273 strength of the covariate. The Kolmogorov-Smirnov test of CSR (Complete Spatial
274 Randomness) and Berman's Z_2 statistics were used to test the strength of evidence for
275 a covariate effect. The Receiver Operating Characteristic (ROC) plot, and the area
276 under the ROC curve (AUC), closely related to Berman's Z_2 test, measure the magni-
277 tude of the covariate effect. AUC values close to 1 or 0 indicate strong discrimination,
278 whereas intermediate values (0.5) suggest no discrimination power.

279 Whereas intensity is a first-order property of the point process, multiscale inter-
280 point interaction is measured by second or higher-order moment quantities, such as
281 the Ripley's K correlation function (Ripley, 1976, 1977) and the distance G -, F - and
282 J -functions. Three different types of inter-point interaction are possible: random, reg-
283 ular or cluster. Regular patterns are assumed to be the result of inhibition processes,
284 while cluster patterns are the result of attraction processes. In order to reduce the
285 edge effect bias in estimating the correlation between points, we implemented Rip-
286 ley's isotropic edge correction (Ohser, 1983; Ripley, 1988). In a hypothesis-testing
287 framework, pointwise envelopes were computed by 199 random simulations of the
288 null hypothesis. Thus, values of the empirical distribution (black solid line) were plot-
289 ted against the benchmark value (red dotted line) and the envelopes (grey area) which
290 specify the critical points for a Monte Carlo test (Ripley, 1981).

291 In order to test the spatial dependence between remains associated with the ero-
292 sional event of UB4c and those associated with the underlying UB5a unit, we treated
293 the data as a multivariate point pattern, assuming that the point patterns in UB4c and
294 UB5a are expressions of two different stationary point processes, i.e., depositional
295 events. We performed a cross-type pair correlation function ($g_{ij}(r)$), derivative of the
296 multitype $K_{ij}(r)$ function, which is the expected number of points of type j lying at a
297 distance r of a typical point of type i . The function is a multiscale measurement of the
298 spatial dependence between types i (UB4c) and j (UB5a). Randomly shifting each of
299 the two patterns, independently of each other, estimated values of $\hat{g}_{ij}(r)$ are compared
300 to a benchmark value $g_{ij}(r) = 1$, which is consistent with independence or at least with
301 lack of correlation between the two point processes.

302 In addition to the pair correlation function, the multitype nearest-neighbour $G_{ij}(r)$
303 function was used to estimate the cumulative distribution of the distance from a point of
304 type i (UB4c) to the nearest point of type j (UB5a). It measures the spatial association
305 between the two assemblages. For the cross-type G -function, the null hypothesis states
306 that the points of type j follow a Poisson (random) distribution in addition to being
307 independent of the points of type i . Thus, in a randomisation technique, when the solid
308 line of the observed distribution ($\hat{G}_{ij}(r)$) is above or below the shaded grey area, the
309 pattern is significantly consistent with clustering or segregation, respectively. Complete
310 spatial randomness and independence (CSRI) of the two point processes would support
311 an exogenous origin hypothesis for the assemblage recovered from the UB4c unit. On
312 the other hand, positive or negative association can be interpreted as expression of
313 different endogenous processes.

314 The particle size spatial distribution of the lithic assemblage from UB4c was inves-
315 tigated by means of a transformation of the multitype K -function ($K_{i\bullet}(r) - K(r)$, see
316 [Baddeley et al. \(2015\)](#), p.608). In this case, we treated the data as the manifestation of a
317 single multitype point process. In a joint distribution analysis, the locations and types
318 of points are assumed to be generated at the same time. The null model of a random
319 labelling test states that the type of each point is determined at random, independently
320 of other points, with fixed probabilities. The estimated K -function for a subset of pos-
321 sible combinations was evaluated against the envelope of Monte Carlo permutations of
322 the class of remains. Likewise with the vertical distribution, a horizontal clustering of
323 small specimens, such as lithic debris/chips, together with larger dimensional classes
324 of remains would suggest the lack of sorting by natural depositional processes and a *en*
325 *mass* model of deposition.

326 As for the three-dimensional distribution of the lithic artefacts in Area A, and their
327 spatial association with the partial skeleton of the *E. (P.) antiquus*, we applied three-
328 dimensional univariate and bivariate second-order functions. A rectangular box of 20
329 square meters and 80 cm vertical extent was selected for the analyses (green outline in
330 Fig. 9a). Assuming homogeneity, the univariate pair correlation function ($g_3(r)$) was
331 estimated for the pattern of all the artefacts (mostly debris/chips) from UA3c and UA4.
332 In the specific context of the site, complete spatial randomness (CSR) would suggest

Table 3: Global tests for circular uniformity

Sample	mean dir.	Rayleigh		Kuiper		Watson		Rao		level
		\bar{R}	p - value	test	critical value	test	critical value	test	critical value	
UA3c	77.17°	0.268	0.029	2.4698	2.001	0.2967	0.267	271.8367	160.53	0.01
UA4	35.79°	0.386	0.003	2.5656	2.001	0.3437	0.267	246.3158	163.73	0.01
<i>E. (P.) antiquus</i>	54.64°	0.489	2.775e-07	3.4811	2.001	0.906	0.267	291.4286	155.49	0.01
UB4c (clock)	83.96°	0.167	0.091	2.327	2.001	0.2466	0.267	309.7674	155.49	0.01
UB4c (compass)	128.14°	0.225	0.037	1.6917	2.001	0.1862	0.267	153.3846	155.49	0.01

that the pattern most probably is the result of a random distribution process, such as a high energy mass movement. In contrast, other natural processes would produce clustering or segregation of the lithic artefacts. Spatial aggregation, if not generated by obstructions, would support an *in situ* primary origin of the assemblage.

In support to the pair correlation function, the cross-type nearest-neighbour function has been applied in order to compute, for each artefact recovered from the UA3c and UA4 units, the nearest point associated with the elephant skeleton. A prevalence of short distances would indicate aggregation of the lithic artefacts around the mass of the elephant; whereas a uniform or symmetric distribution would support random independent processes.

4. Results

4.1. Fabric analysis

The rose diagrams in Fig. 4 visualise the circular distributions of the examined specimens. Overall, the UA4 sample and the sample of elephant bones show predominant peaks in the NE quadrant; while the ones from units UA3c and UB4c suggest uniform to multimodal distributions. Specifically, the UA4 sample distribution (Fig. 4b) spreads largely in the NE quadrant. Similarly, the circular distribution of the elephant sample (Fig. 4c), mainly lying in UA4, resembles the former distribution: it is skewed to the SW and concentrated in the NE quadrant. On the other hand, the UA3c sample (Fig. 4a) and the two samples from Area B (Fig. 4d,e) suggest a different isotropic scenario.

Table 3 summarises the results of the circular uniformity tests. With regard to the UA3c sample, the Rayleigh test ($p - value = 0.029$) rejected the null hypothesis of

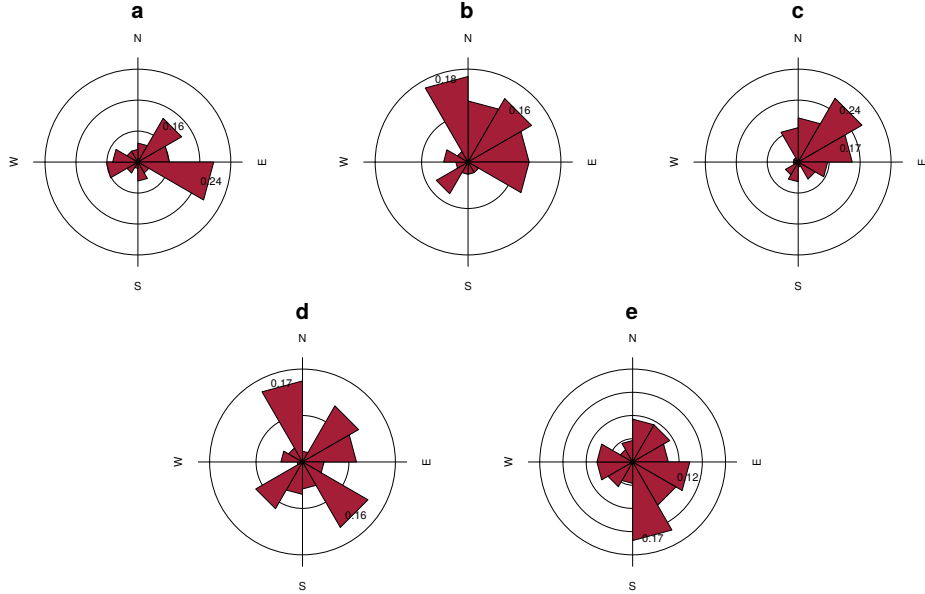


Figure 4: Rose diagrams showing the bearing patterns of samples from UA3c (a), UA4 (b), the elephant carcass (c) and UB4c (d: clock method, e: compass method)

356 circular uniformity. The mean resultant length ($\bar{R} = 0.268$) and the mean direction
 357 of 77.17° are thus significant, assuming the distribution is unimodal. However, the
 358 Kuiper, Watson and Rao omnibus tests also rejected the null hypothesis of uniformity,
 359 therefore suggesting multimodal anisotropy in the distribution, as shown by the rose
 360 diagram (Fig. 4a).

361 For the UA4 sample and the subset of elephant bones, all the tests agreed in reject-
 362 ing the null hypothesis in favour of a preferentially oriented distribution. The Elephant
 363 sample, with respect to the other, showed stronger anisotropy and significantly higher
 364 \bar{R} . As suggested by the rose diagrams (Fig. 4c), this sample has a mean direction to-
 365 wards the NE (55°) and relatively low circular variance (29°).

366 The UB4c sub-samples had discordant test results when considering the Rayleigh
 367 and the omnibus statistics. According to the Rayleigh test, the mean resultant length
 368 (\bar{R}) and the mean direction were not significant for the sub-sample of measurements
 369 recorded with the clock system. Conversely, a weak significant test result was obtained
 370 for the sub-sample of measurements recorded using the compass. Overall, for the latter

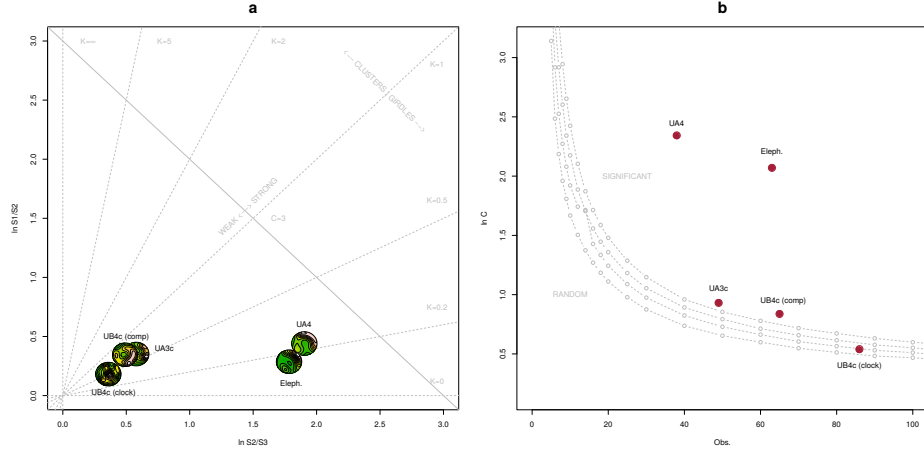


Figure 5: Woodcock's eigenvalues ratio graph (a) and plot of the Monte-Carlo critical S_1/S_3 test values, for varying sample sizes and confidence levels (b), modified from [Woodcock and Naylor \(1983\)](#).

371 sub-sample all the omnibus tests suggested significant isotropy (Fig. 4e). On the other
 372 hand, the Kuiper and Rao tests, suggested a multimodal departure from uniformity for
 373 the sample recorded using the clock method (Fig. 4d).

374 The results obtained for the UA3c sample and the UB4c sub-sample recorded using
 375 the clock method are most probably due to the shape of those distributions. Indeed, the
 376 clock system, being less accurate, tends to produce a less dense distribution, more
 377 subject to show a multimodal shape when the distribution is actually uniform (Fig. 4a,
 378 d).

379 The Woodcock eigenvalues ratio graph (Fig. 5a) presents the shape (K) and strength
 380 (C) of the distributions. Fig. 5b plots confidence levels of Monte-Carlo critical C val-
 381 ues, varying for sample sizes. The two samples from Area B, together with the UA3c
 382 sample, having low C values, plotted close to the origin of the ratio graph. Thus, they
 383 suggest nearly significant randomness. On the other hand, the UA4 and the elephant
 384 samples, with higher C values, showed a stronger and significant tendency to orient
 385 preferentially. The shape parameter K of the samples varied from $K = 0.7$ for the
 386 UB4c sample measured with the compass to $K = 0.1$ for the elephant sample. Overall,
 387 all the samples plotted below the average shape value ($K = 1$) between girdles and
 388 clusters distributions.

389 The Benn diagram (Fig. 6) resembles the Woodcock ratio graph (Fig. 5a). The
390 samples from units UB4c and UA3c clearly plotted at a distance from the UA4 and the
391 elephant samples. The UB4c sub-sample of measurements recorded with the compass,
392 together with the UA3c sample, plotted in the centre of the ternary graph. As shown
393 above, the UB4c sub-sample of measurements taken using the clock system exhibited
394 more isotropy.

395 Compared to the ranges recorded for modern natural processes (debris flow, runoff,
396 solifluction), the fabric from the UA3c and UB4c units plotted well inside the cluster of
397 debris flows, with the UB4c (clock) sample suggesting even more random orientations.
398 On the other hand, the sample of elephant remains, which lie mostly on UA4 and are
399 covered by UA3c, plotted significantly close to the sample from unit UA4. They both
400 presented the lowest isotropy index (*IS*), but not high elongation index (*EL*). Thus,
401 they plotted in the average between linear and planar orientations, within the range of
402 runoff processes. Yet they still plotted at the margins of the cluster of debris flows
403 fabrics. Moreover, the elephant sample showed a more planar attitude with respect to
404 the UA4 sample.

405 *4.2. Vertical distribution*

406 Fig. 7 compares the distribution of the absolute elevations of the partial skeleton of
407 the *Elephas (P.) antiquus* with the other remains from Area A. Overall, the vertical dis-
408 tribution of the elephant approximates a normal distribution with mean (μ) 349.25 m
409 a.s.l. and standard deviation (σ) 0.12 m. The mean elevation of the erosional con-
410 tact between the two stratigraphic units is slightly above the latter ($\mu = 349.30$ m).
411 Although difficult to quantify due to its not sharp nature, the range of elevations of
412 this contact, as estimated from the IDW interpolation (Fig. 3a), is relatively small
413 ($\sigma = 0.06$ m).

414 Three lithic artefacts (two flakes and one tool) from the UA3c unit are located
415 within its positive half. Only one flake has been found in the lower UA4, at about
416 349.10 m, together with three chips. However, they plotted well within the left tail
417 of the debris/chip distribution from the unit above. Despite the scarcity ofdebitage
418 products in this area, waste products (debris/chip) are relatively well represented (16%

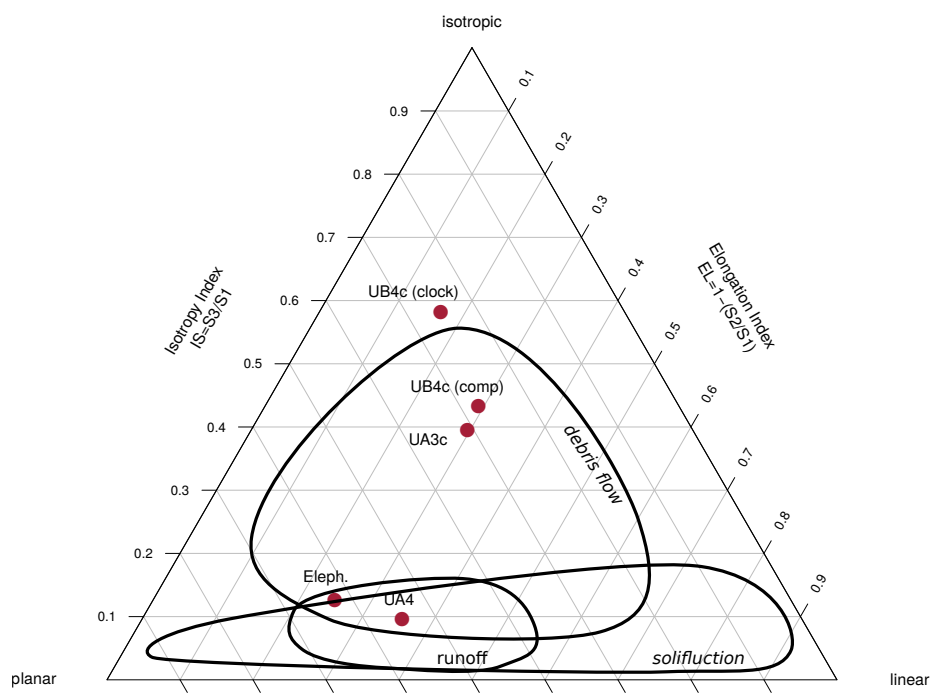


Figure 6: Benn's diagram. Fabric ranges of natural processes modified from Bertran et al. (1997); Lenoble and Bertran (2004).

419 of the UA3c sample). Their vertical distribution approximates a normal distribution
420 ($\mu = 349.50$ m and $\sigma = 0.18$ m), having almost 50% of the sample in the range of
421 elevations of the erosional surface and the rest above it. Notably, the distribution of
422 the faunal remains from the same unit resembles that of the debris/chip. The Welch
423 two sample t-test ($p - value = 0.5099$) failed to reject the null hypothesis that the
424 two population means are equal. On the other hand, the vertical distribution of faunal
425 remains recovered from the UA4 unit is comparable with that of the *Elephas* ($p -$
426 $value = 0.6562$). Nevertheless, the density functions altogether clearly confirm one
427 of the main observations assessed during excavation, namely that the elephant remains
428 and most of the recovered faunal and lithic material in Area A lie at or close to the
429 UA3c/4 contact, with unit UA3c covering the remains.

430 Fig. 8 shows the empirical density functions of the minimum distances from each
431 specimen from Area B to the UB4c/5a erosional contact (Fig. 3b). The combined
432 distribution of any type of find from the UB5a unit (Fig. 8a) skewed to the left with
433 a short tail (up to -0.3 m). The mode, between 5 and 10 cm below the roof of UB5a,
434 indicates a general concentration of material very close to the contact of this unit with
435 the overlying UB4c, in accordance with the mean distribution of the different classes of
436 remains. Although the majority of both the lithic and faunal assemblages were found
437 in the uppermost 15 cm of UB5a, few debris/chips and bone fragments occur lower
438 in the sequence, yet no more than 30 cm below the roof of this unit. Very few flakes,
439 three tools and no cores have been found in this unit. As a whole, the lithic assemblage
440 from UB5a, mostly composed by debris/chips, is only 7% of the most conspicuous
441 assemblage from UB4c.

442 The global distribution of unit UB4c was right skewed (up to almost 0.6 m) and cen-
443 tred at about 5 cm above the contact with the underlying unit UB5a (Fig. 8b). Almost
444 30% of the sample fell exactly at the erosional contact that separates UB4c from UB5a.
445 The density estimations of the lithic debris/chip, flakes, tools and faunal remains sig-
446 nificantly overlap, whereas the distribution of the six cores shows a bimodal shape with
447 peaks at 5 and 20 cm above the contact. However, the Welch Two Sample t-test of the
448 lithic and faunal sample means failed to reject the null hypothesis ($p - value = 0.6295$).

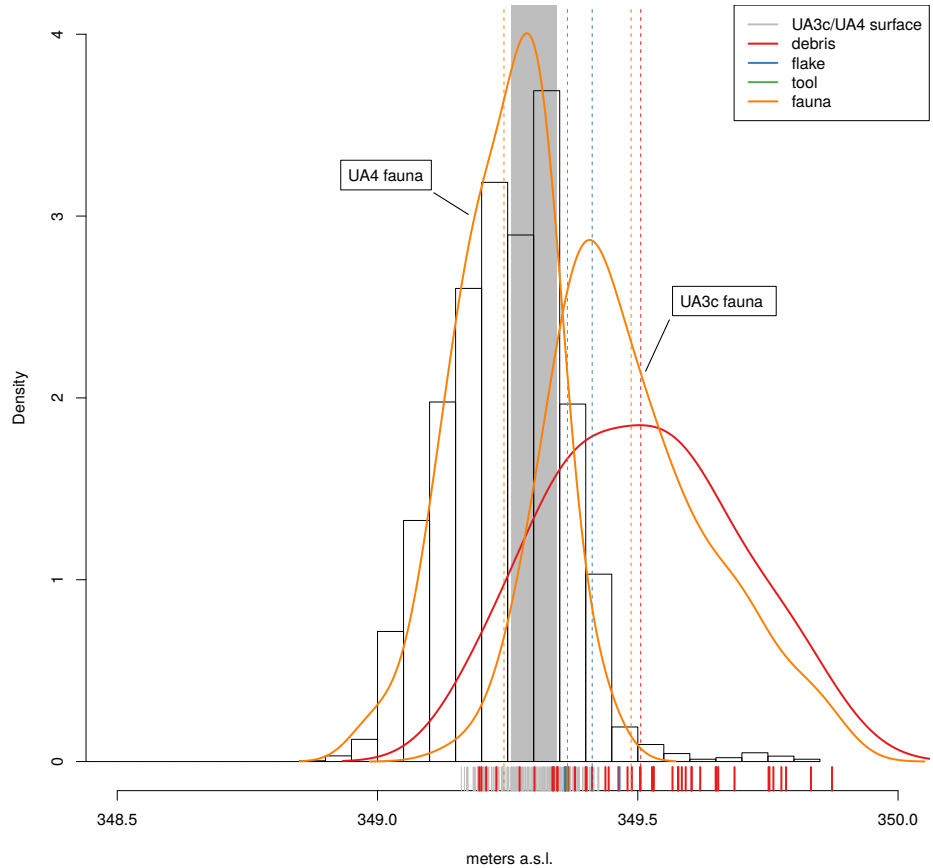


Figure 7: Empirical density functions of absolute elevations (meters a.s.l) of remains from Area A. The histogram represents the *Elephas (P.) antiquus* range of elevations; the grey area shades the $Q_3 - Q_1$ range of the erosional UA3c/4 surface; dashed lines indicate mean values.

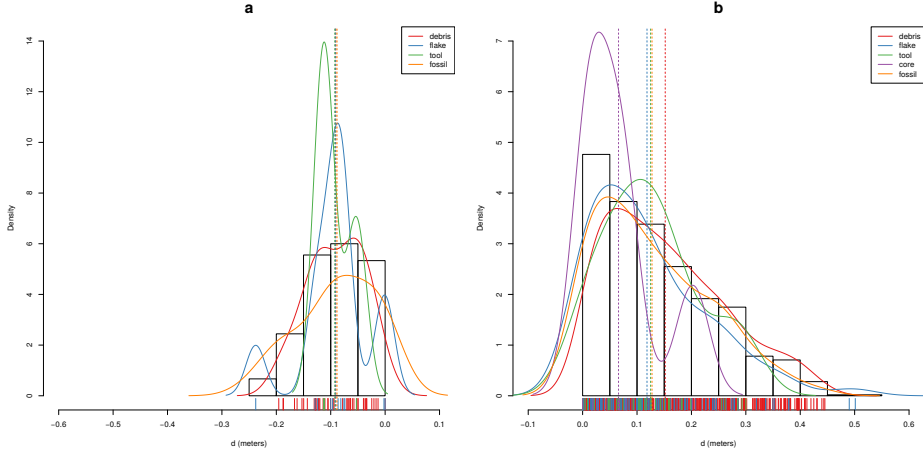


Figure 8: Empirical density functions of minimum orthogonal distances (d) to the UB4c/5a surface. The histogram represents the total distribution of remains from UB5a (a) and UB4c (b); dashed lines indicate mean values.

449 **4.3. Point pattern analysis**

450 Results of the point pattern analysis are complementary to those obtained from the
451 analysis of the vertical and fabric distributions.

452 Regarding Area A, kernel density estimation and three-dimensional functions were
453 applied in order to quantitatively depict the spatial distribution of the lithic assemblage
454 in relation to the elephant skeleton.

455 Fig. 9a shows the smoothing kernel intensity estimation of the combined lithic and
456 faunal assemblage from the UA3c unit. Contour lines delimit the density of the lithic
457 sample. The partial skeleton of the *E. (P.) antiquus* is superimposed on it. A pre-
458 liminary visual examination of the plot suggests a homogeneous distribution of lithics
459 (mostly debris/chips) and fossils. Spots of higher density appear to be spread around
460 and in association with the elephant remains.

461 The univariate pair correlation function of the joined lithic assemblage from the
462 UA3c and UA4 units (Fig. 9b) suggests aggregation of finds. The estimated $\hat{g}_3(r)$
463 function (black solid line) wanders above the benchmark value (red dotted line) until
464 values of $r = 0.8$. However, for distances between 35 and 65 cm, it lies above the
465 grey envelope of significance for the null hypothesis of CSR, indicating that at those

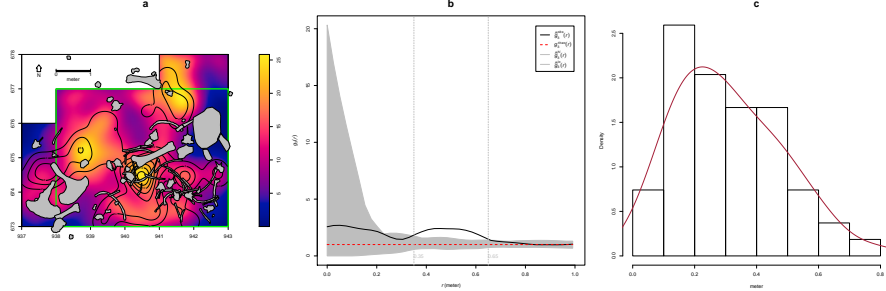


Figure 9: Kernel smoothed intensity function of the lithic and faunal assemblages from UA3c. Isolines mark the density of the lithic artefacts (a). Pair correlation function ($g_3(r)$) of a three-dimensional pattern of lithic artefacts from UA3c and UA4. Grey envelope of 999 Monte Carlo simulations under the CSR null hypothesis (b). Three-dimensional distance from each lithic artefact from UA3c and UA4 to the nearest neighbour elephant remain (c).

distances artefacts occur closer than expected in the case of random processes. For values of $r > 0.8$, the function stabilises at values close to 0, suggesting a Poisson distribution. The plot illustrates the random distribution of finds between patches of clusters that we observe in the kernel density estimation (Fig. 9a).

The histogram in Fig. 9c shows the density of the distances calculated from each artefact to the nearest-neighbour elephant remain. A right skewed distribution, with a prevalent peak at 10 cm and mean μ 30 cm is an indication of the relatively strong aggregation of events around the mass of the elephant skeleton.

As for Area B, the analysis first focused on the spatial distribution and cross-correlation of the assemblages from UB4c and UB5a (Fig. 10); and secondly on the interaction between classes of remains from UB4c (Fig. 11).

Figs. 10a,b respectively show kernel density estimations of the combined lithic and faunal assemblages from both the units analysed. Despite the samples size difference, a first visual examination suggests the presence of interesting spatial structures.

Regarding the UB4c unit (Fig. 10a), the high density of material concentrated around the western square 934/600 suggests that the pattern could have been the result of an inhomogeneous, non-uniform depositional process. Visual comparison of the density plot with the elevation model of the erosional contact between the UB4c

and UB5a units (Fig. 3b) suggests positive correlation between lower elevations (topographic depressions) and higher density of remains. Fig. 10c shows the results of the ρ -function, which estimates the intensity of the UB4c sample assemblage as a function of the covariate underlying topography created by the erosional event. Within the range of elevation between 350.2 and 350.4 m, the occurrence of finds is higher and the intensity decreases with the rise of elevation, i.e., finds are more likely to be found at lower elevations than would be expected if the intensity was constant.

Spatial Kolmogorov-Smirnov and Berman's Z_2 (Berman, 1986) statistics were used in order to test the dependence of the UB4c pattern on the covariate erosional surface. Both KS ($D = 0.11952$, $p - value = 7.772e - 16$) and Z_2 ($Z2 = -7.8447$, $p - value = 4.34e - 15$) significantly rejected the null hypothesis of CSR. Although the tests suggested evidence that the intensity depends on the covariate, the effect of the covariate is weak and it seems to have no discriminatory power. The ROC curve and AUC statistics (0.56), which measure the strength of the covariate effect, suggest that the underlying UB4c/5a topography does not completely explain the localised high density of occurrence in the UB4c.

Relative spatial segregation seems to occur between the assemblages from UB4c (Fig. 10a) and UB5a (Fig. 10b), with high density of the former distribution corresponding to low density of the latter. The former analysis of the vertical distribution showed that the two assemblages occur very close to their stratigraphic contact. In order to further investigate the spatial interaction between the two depositional events, we applied multitype pair correlation ($g_{ij}(r)$) and nearest-neighbour ($G_{ij}(r)$) functions.

Fig. 10d shows the estimated values of the multivariate $\hat{g}_{ij}(r)$ function against the envelope of the null hypothesis, obtained by randomly shifting the position of remains from the two distributions in 199 Monte Carlo simulations. For fixed values of r less than 30 cm the observed function lies below the benchmark value of independence, thus indicating segregation; but it wanders at the lower edge of the grey envelope. For fixed distances of $r > 0.3$ m the observed and theoretical lines significantly overlap. Overall, the function suggests independence of the two point processes (UB4c and UB5a) at multiple scales.

However, the estimated $\hat{G}_{ij}(r)$ function (Fig. 10c), running well below the signifi-

515 cance grey envelope for fixed values of $r > 0.3$ m, confirms that the nearest-neighbour
516 distances between remains from UB4c and UB5a are significantly longer than expected
517 in the case of independent processes. Interestingly, at values of $r < 0.2$ m the observed
518 function failed to reject the null hypothesis of Complete Spatial Randomness and In-
519 dependence (CSRI).

520 With the aim to integrate the vertical distribution analysis, the particle size spatial
521 distribution of remains from the UB4c unit were investigated by means of a deriva-
522 tive of the multitype K -function, randomly labelling the classes of remains. Fig.11
523 shows a selection of the array of possible combinations between classes. In any panel,
524 the estimated function wanders above the benchmark value. Such positive deviations
525 from the null hypotheses suggest that debris/chips are more likely to be found close
526 to the other class of remains than would be expected in case of a completely random
527 distribution. Permutating the lithic debris/chips with flakes (Fig.11a), tools (Fig.11b),
528 cores (Fig.11c) and faunal remains (Fig.11d), the Monte Carlo test results would have
529 been significantly consistent with clustering, if we had chosen distance values $r > 0.4$,
530 $r > 0.4$, $r > 0.9$, $r > 0.8$, respectively. Conversely, we could not reject the null
531 hypothesis of CSRI for lesser values of r .

532 **5. Discussion**

533 Recent excavations at the Middle Pleistocene site of Marathousa 1 have unearthed
534 in one of the two investigated areas (Area A) a partial skeleton of a single individual of
535 *Elephas (P.) antiquus*, whose bones are in close anatomical association, and spatially
536 and stratigraphically associated with lithic artefacts and other faunal remains. In Area
537 B, about 60 m to the South of Area A, we collected a much higher number of lithic
538 artefacts (Tourloukis et al., this volume), spatially and stratigraphically associated with
539 other faunal remains, including isolated elephant bones, cervids and carnivores among
540 others (Konidaris et al., this volume).

541 The two areas are stratigraphically correlated, the main fossiliferous layers (UA3c
542 and UB4c) representing a relatively low-energy depositional process, such as a hyper-
543 concentrated flow that dumped material in a lake margin context (Karkanas et al., this

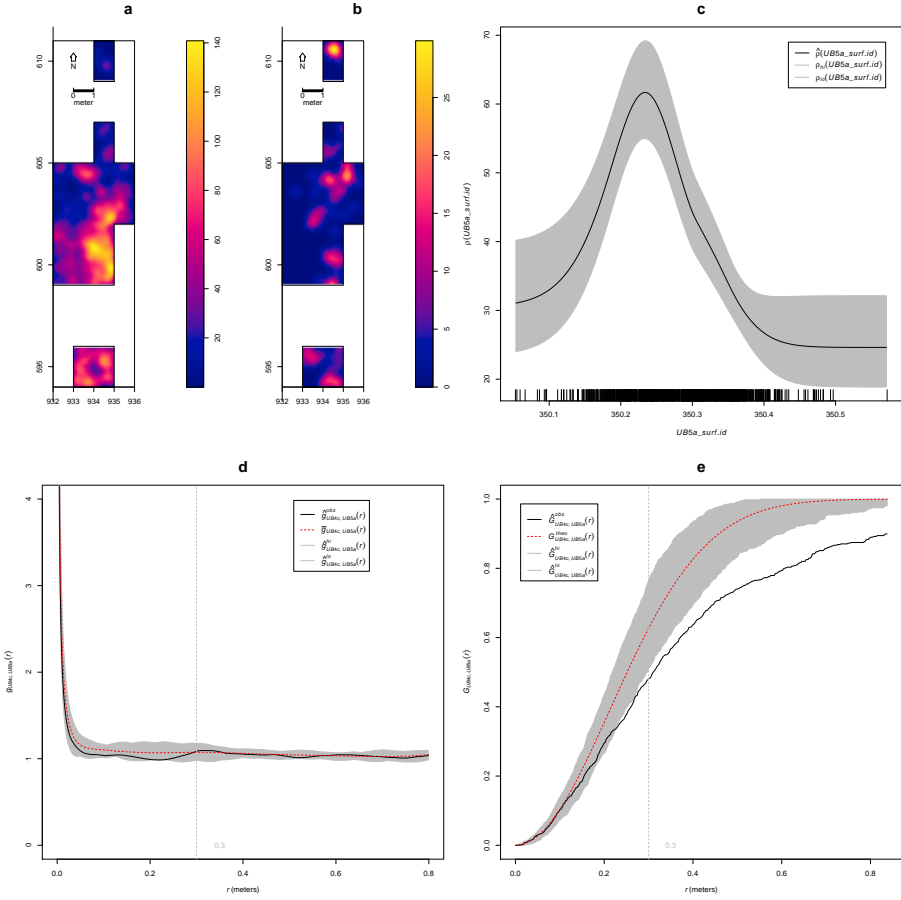


Figure 10: Kernel smoothed intensity function of the lithic and faunal assemblages from UB4c (a) and UB5a (b). Smoothing estimate of the intensity of remains from UB4c, as a function of the erosional surface UB4c/5a. Grey shading is pointwise 95% confidence bands (c). Cross-pattern pair correlation function ($g_{ij}(r)$) between the UB4c and UB5a distributions. Grey envelope of 199 Monte Carlo simulations under the independence of components null hypothesis (d). Multitype nearest-neighbour function ($G_{ij}(r)$) between the UB4c and UB5a distributions (e).

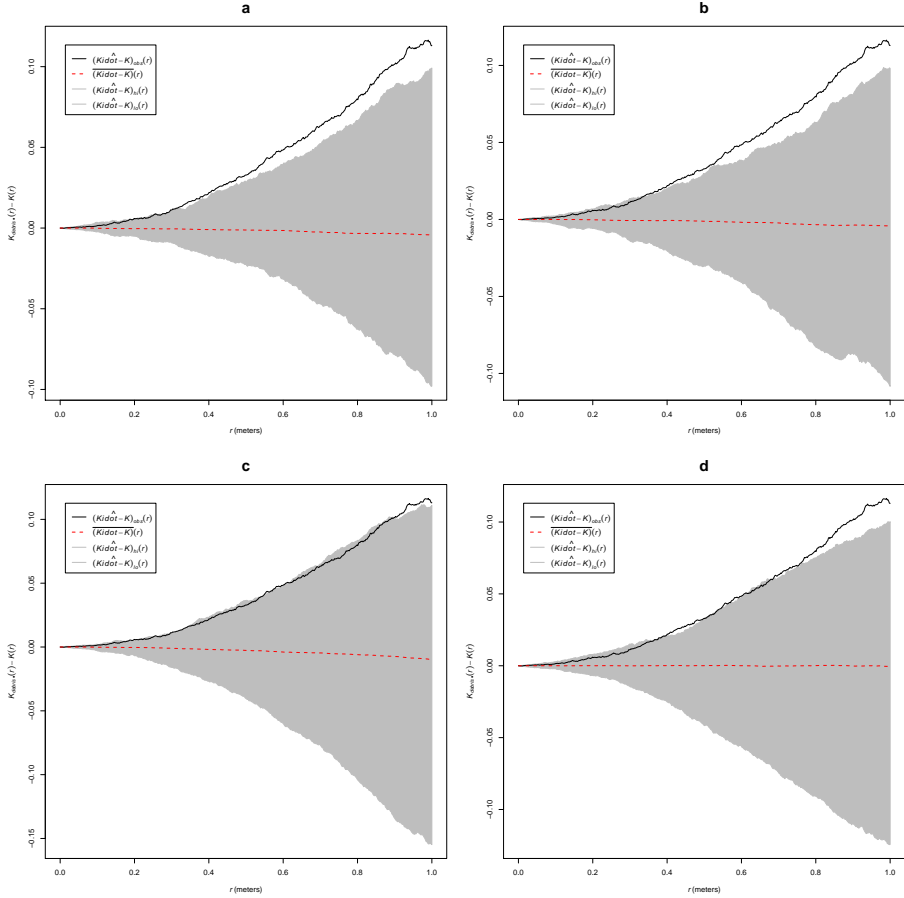


Figure 11: Random labelling test for the UB4c assemblage. Grey pointwise envelope of 199 Monte Carlo permutation of debris/chips with flakes (a); tools (b); cores (c); fossils (d).

544 volume).

545 To date, evidence of butchering (cut-marks) has been identified on two bones of
546 the elephant skeleton from Area A, as well on elephant and other mammal bones from
547 Area B (see Konidaris, this volume).

548 However, due to the secondary deposition nature of the main fossiliferous horizon,
549 it is of primary importance to evaluate the degree and reliability of the spatial
550 association of the lithic artefacts with the faunal remains, and especially with the ele-
551 phant skeleton. In order to tackle our main objective, we applied a comprehensive
552 set of spatial statistics to the distributions of the archaeological and zooarchaeologi-
553 cal/palaeontological remains from relevant stratigraphic units of the two areas of in-
554 vestigation. Preliminary results are here discussed for both areas.

555 *5.1. Fabric analysis*

556 The analysis of the orientation (dip and strike) of subsets of remains, mostly bone
557 fragments, organic residues and lithic artefacts, showed different patterns for the two
558 main find-bearing units.

559 The test results (Tab. 3) for the UA4 sample and the sample of elephant remains
560 - which lie on unit UA4 and are covered by UA3c - indicated significant preferential
561 orientations towards the NE (Figs. 4b,c). As shown by the Woodcock's (Fig. 5) and the
562 Benn's diagrams (Fig. 6), these samples plotted together at a distance from the others.
563 Such convergence suggests that the elephant carcass, the other faunal remains and the
564 organic material, deposited on unit UA4, were subjected to the same processes.

565 Far from the isotropic corner in the Benn's diagram these two samples from Area
566 A plotted almost in between the linear and planar extremes, with the elephant sample
567 showing a more planar fabric. When the results published by Bertran et al. (1997) and
568 Lenoble and Bertran (2004) from observations of fabrics in modern subaerial slope
569 deposits were used as a reference, the two samples aggregated well within the cluster
570 of runoff process. Yet they still plotted at the extreme margins of debris flow and
571 relatively distant from the linear corner.

572 This result is consistent with the exposure of unit UA4 to overland water-laden
573 processes that occurred before the flood event UA3/UB4 (Karkanas et al., this vol-

ume). Notably, the erosive nature of low-energy processes triggered by rain-water has been observed on lacustrine floodplains, and is associated with anisotropic patterns in autochthonous assemblages (Cobo-Sánchez et al., 2014; Domínguez-Rodrigo et al., 2014c; García-Moreno et al., 2016).

On the other hand, the fabric of the UA3c sample, being similar to those of the UB4c sub-samples (Figs. 5 and 6), supports the stratigraphic correlation between these units across the two investigated areas. The fabric analysis suggests that the UA3/UB4 process can be categorized as a flood event, which falls in the spectrum between debris and hyperconcentrated flow. Indeed, random distribution and orientation of clasts is expected for debris flows, except at flow margins, where preferential orientation and clusters of clasts have been observed (Pierson, 2005). Eventually, such flood would have had the power to significantly reorient elements of the elephant carcass and slightly displace them.

Unlike bones with a tubular shape (i.e., long bones), ribs and vertebrae are prone to orient preferentially under high energy processes, less likely under low energy processes (Domínguez-Rodrigo and García-Pérez, 2013; Domínguez-Rodrigo et al., 2014c). Interestingly, whereas some of the ribs share the same preferential orientation with the long bones, others are oriented NW/SE. However, a NW/SE orientation could be consistent with a prevalent NE direction of the flow (and vice-versa), since long bones could roll orthogonally to the flow direction (Voorhies, 1966).

On the other hand, a higher energy flood would lead to an under-representation of most cancellous grease-bearing bones, which are prone to be easily transported by water induced processes (Voorhies, 1966). Yet several carpals, tarsals, metapodials, phalanges, ribs and vertebrae are present and in close spatial association with the elephant cranium and other skeletal elements.

The presence of many of the skeletal elements suggests that the elephant carcass was not subjected to high energy processes. Thus, we can assume that relatively low energy overland flows slightly reworked and oriented the exposed elements of the already dismembered (and probably already marginally displaced) elephant carcass, which mostly preserves close anatomical associations, but not anatomical connections.

In Area B, two sub-samples from the same stratigraphic unit were analysed, accord-

ing to the different methods used for recording the orientation (dip and strike) of the finds (i.e., 'clock' vs. compass), mostly faunal remains, wood fragments and lithic artefacts. Due to the different shapes of the two distributions (Figs. 4d,e), test statistics reported contrasting results (Tab. 3). Indeed, the clock system, recording non-continuous circular data, tends to produce a distribution more subject to show a multimodal shape when the distribution is actually uniform. However, the three-dimensional Woodcock (Fig. 5) and Benn (Fig. 6) diagrams agreed upon assessing the randomness of the samples. Despite minor differences between the two samples, both plotted with the UA3c sample in the reference range of debris flows.

5.2. Vertical distribution

As for the vertical distribution, we assume that mass wasting processes, such as debris or hyperconcentrated flows, would predominantly distribute extremely poorly sorted clasts homogeneously throughout the sequence. Normal or inverse grading can be observed in such flows (Pierson, 2005). A concentration of unsorted elements in the proximity of the erosional surface, as well as the absence of any grading, would in turn suggest an autochthonous assemblage.

The lithic assemblage from Area A - the combined sample from units UA3c and UA4 ($n = 54$), composed by a fewdebitage products and a relatively high number of debris/chips and retouch waste products (Tab. 2) - plotted predominantly in the proximity of the erosional surface created by the UA3/UB4 event. The faunal remains from unit UA3c resemble the distribution of the archaeological assemblage as a whole; whereas the ones from the underlying unit UA4 match the vertical distribution of the elephant (Fig. 7).

Overall, the material recovered from unit UA3c did not show any grading and mainly plotted at the bottom of the unit, thus consistent with the hypothesis of an autochthonous assemblage.

In Area B, two samples from units UB4c ($n = 1243$) and UB5a ($n = 101$) respectively, were analysed (Tab. 2), for quantifying the minimum orthogonal distance of each item to the modelled erosional surface (Fig. 3b).

634 The vertical distribution of lithic artefacts and fossils from unit UB4c showed a pre-
635 dominant peak right at the contact with the erosional surface. Almost 30% of this rich
636 sample plotted at a distance between 0 and 5 cm from the erosional contact; whereas
637 the rest gently skewed to the upper part of the unit, up to about 50 cm. The same distri-
638 bution was observed for all classes of remains, suggesting no size sorting and an origin
639 very close to the erosional surface (Fig. 8b).

640 The density distribution of the sample from the underlying UB5a unit (Fig. 8a)
641 globally indicates a more constrained vertical displacement of remains (within 30 cm
642 below the erosional surface). Whereas lithic artefacts and fossils mostly plot right at
643 the contact and just below it, a few debris/chips and faunal remains were found lower
644 in the sequence. No size sorting was observed, but, notably, lithic cores are absent and
645 the debris/chip distribution is wider than the distribution of the few flakes and tools.

646 Field observations of cracks in the clayey UB5a unit testify shrinking and swelling
647 during wetting and drying cycles (Karkanas et al., this volume), which suggests that
648 vertical displacement of some small lithics and fossil fragments at lower depths with
649 respect to the UB5a/4c contact probably resulted from clay desiccation.

650 Likewise, [Lenoble and Bertran \(2004\)](#) documented up to 30 cm vertical dispersion
651 and frequent vertical dip of artefacts from the marshy silty clay of the Croix-de-Canard
652 site, sector 3.

653 Furthermore, a recent experimental study of animal trampling in water saturated
654 substrates reported negative correlation with artefact size, significant inclination and
655 greater vertical displacement than any former work: a maximum between 16 and
656 21 cm, with a mean of about 6 cm ([Eren et al., 2010](#)).

657 The fact that the majority of the remains from units UB4c and UB5a plotted at
658 or very close to the contact between these two layers, the relatively high percentage
659 of lithics in both units, as well as the absence of size sorting or grading, suggest au-
660 tochthonous assemblages, deposited in UB5a and subsequently eroded *in situ* by the
661 UA3/UB4 flood event.

662 5.3. Point pattern analysis

663 The hypothesis that in both areas the lithic and faunal assemblages were primarily
664 deposited *in situ* and were subsequently somewhat reworked by a low energy flood,
665 was further explored by means of point pattern analysis.

666 We assumed that a completely random spatial distribution of the lithic artefacts
667 and faunal remains would suggest an allochthonous origin and subsequent transport to
668 the site by the action of a random massive process, such as debris flow. Nevertheless,
669 clustering of artefacts is not necessary evidence for human presence. Aggregation or
670 segregation patterns could be produced by a range of biotic and/or natural processes.
671 Human activities, topography and physical obstructions alike could trigger spatial ag-
672 gregation.

673 The three-dimensional distribution of lithic artefacts from unit UA3c shows signif-
674 icant clustering for values of r between 35 and 65 cm. Lithic artefacts occur relatively
675 close to the skeletal elements of the elephant, mostly about 20 cm apart and not more
676 than 50 cm apart (Fig. 9). The richest cluster of about 20 lithic artefacts is located SW
677 of the cranium, close to the right femur and the scatter of ribs and vertebrae.

678 Considering the prevalent NE orientation of the elephant bones and the other faunal
679 remains from UA4, it is not unlikely that a SW/NE oriented flood could have been
680 responsible for the observed accumulation SW of the elephant cranium, which would
681 have represented an important obstruction to the flow. A similar case of clustering of
682 small remains, apparently dammed by a long elephant tusk, has also been observed at
683 Castel di Guido ([Boschian and Saccà, 2010](#)).

684 As mentioned above, whereas fairly random fabric and spatial distribution of coarse
685 clasts are observed at the centre of modern debris flow deposits, preferential orientation
686 and clustering may occur at the margin of the flood ([Pierson, 2005](#)). Yet the fabric
687 analysis of the UA3c sample shows a random distribution, which falls within the range
688 of debris flow (Fig. 6), and the pair correlation function (Fig. 9b) suggests significant
689 clustering of lithic artefacts at relatively small scale: a pattern less likely to be produced
690 by a large scale massive process such as a debris flow. Moreover, clusters of lithic
691 artefacts occur as well in areas with less density of elephant bones.

692 Small scale clustering; proximity to the elephant remains and the erosional surface;

absence of spatial size sorting and, on the contrary, the presence of a relatively high number of lithic debris/chips associated with some flakes and tools; close anatomical spatial association of the elephant skeletal elements, slightly displaced and preferentially oriented: these lines of evidences support the hypothesis of an autochthonous primary deposition, subject to localised minor reworking.

A similar pattern can be observed in Area B, where a first set of spatial statistics confirmed that the inhomogeneous density of remains from unit UB4c (Fig. 10a) is not completely explained by the covariate effect of the underlying complex topography created by the erosional event UA3/UB4 (Fig. 3b).

Thus, we explored the relative spatial interaction between the UB4c and the underlying UB5a samples. We assumed that complete spatial randomness of the two independent depositional processes would occur in case of an exogenous origin and transportation of the UB4c assemblage. The hypothesis of an autochthonous original deposition of the faunal and lithic assemblages on the UB5a unit, subsequently eroded *in situ* by a relatively high energy flood (UB4c), was tested by cross-pattern spatial correlation functions (Figs. 10d,e). Whereas the two samples are vertically adjacent to the erosional surface (Fig. 8), on the horizontal plane they are both more segregated than expected for a random distribution.

Moreover, for the UB4c sample, an unsorted particle size spatial distribution was confirmed (Fig. 11). The occurrence in the same place of small and large classes of remains suggests that post-depositional processes, such as water winnowing, have not severely affected the assemblage. Hyperconcentrated flows would have dumped material on the lake margin. In this way, particles would have been frozen and deposited *en masse*. Hence their non-sorted spatial distribution.

On the other hand, the extraordinary preservation and number of mint to sharp, unsorted lithic artefacts from the UB4c unit; their density, positively correlated to the topography, and significantly segregated from the underlying distribution of remains; the vertical proximity of both assemblages from UB4c and UB5a to the erosional surface; as well as the random orientation pattern of the former, suggest that significant displacement of materials due to the erosional event can be excluded.

The faunal and lithic assemblages from unit UB4c therefore most likely derived

724 from the local erosion of exposed mudflat areas (UB5a layer) and have been slightly
725 redistributed by the same flood event that capped the elephant in Area A.

726 Further evidence that the recovered assemblage has not undergone substantial re-
727 working and has retained its original characteristics would come from the refitting
728 analysis, currently in progress. To date, 4 bone refits have been found in Area B:
729 three from unit UB4c, respectively at 4.771, 0.048 and 0.012 m distance; and one
730 between two mammal bone fragments from units UB4c and UB5a, at a very short dis-
731 tance (0.086 m). Interestingly, one of the elements of the most distant refit (a *Dama*
732 *sp.* mandibular fragment) shows traces of carnivore gnawing (Konidaris et al., this
733 volume).

734 In conclusion, multiple lines of evidence suggest that the erosional event UB4/UA3
735 represents a relatively low-energy process in the continuum between debris and hyper-
736 concentrated flow, which would have locally reworked at a small scale the already
737 exposed or slightly buried and spatially associated lithic and faunal assemblages.

738 Although the UB4/UA3 process represents a snapshot of a relatively short frame of
739 time, inferences about the use of space by human groups, in terms of knapping episodes
740 and butchering activities, are unreliable in light of the current information.

741 The spatial pattern observed at the site is indeed the result of the last in a palimpsest
742 of spatial processes. Whereas the erosional event represented by the debris/hyperconcentrated
743 flow UA3/UB4 caps the sequence and preserves the record, little is known about the
744 eroded underlying occupational horizon.

745 However, whereas hunting or scavenging is still an unsolved matter of debate, con-
746 sidering the bone fragmentation rate, the density of lithic debris/chips, the number of
747 processed bones and their spatial density and association, it is likely that the assemblage
748 represents a complex palimpsest of locally repeated events of hunting/scavenging and
749 exploitation of lake shore resources.

750 More data from high resolution excavations in the coming years would allow us to
751 refine the coarse-grained spatio-temporal resolution of our inferences about past human
752 behaviour at Marathousa 1.

753 **6. Conclusions**

754 At the Middle Pleistocene open-air site of Marathousa 1 a partial skeleton of a
755 single individual of *Elephas (Palaeoloxodon) antiquus* was recovered in stratigraphic
756 association with a rich and consistent lithic assemblage and other vertebrate remains.
757 Cut-marks and percussion marks have been identified on the elephant and other mam-
758 mial bones excavated at the site. The main find-bearing horizon represents a secondary
759 depositional process in a lake margin context.

760 Understanding the site formation processes is of primary importance in order to
761 reliably infer hominin exploitation of the elephant carcass and other animals. To meet
762 this aim, we applied a comprehensive set of multivariate and multiscale spatial analyses
763 in a taphonomic framework.

764 Results from the fabric, vertical distribution and point pattern analyses are consis-
765 tent with a relatively low-energy erosional process slightly reworking at a small scale
766 an exposed (or slightly buried) and consistent scatter of lithic artefacts and faunal re-
767 mains. These results are in agreement with preliminary taphonomic observations of the
768 lithic artefacts (Tourloukis et al., this volume) and the faunal remains (Konidaris et al.,
769 this volume), which also indicate minor weathering and transportation. Our analyses
770 show that multiple lines of evidence support an autochthonous origin of the lithic and
771 faunal assemblages, subject to minor post-depositional reworking. Human activities
772 therefore took place on-site, during an as of yet uncertain range of time.

773 **Acknowledgements**

774 This research is supported by the European Research Council (ERC StG PaGE
775 283503) awarded to K. Harvati. We are grateful to the Municipality of Megalopolis,
776 the authorities of the Region of Peloponnese, and the Greek Public Power corporation
777 (ΔΕΗ) for their support. We also thank Julian Bega and all the participants in the PaGE
778 survey and excavation campaigns in Megalopolis for their indispensable cooperation.

779 **References**

- 780 Anderson, K. L., Burke, A., 2008. Refining the definition of cultural levels at Karabi
781 Tamchin: a quantitative approach to vertical intra-site spatial analysis. *Journal of*
782 *Archaeological Science* 35 (8), 2274–2285.
- 783 Baddeley, A., Chang, Y.-M., Song, Y., Turner, R., 2012. Nonparametric estimation of
784 the dependence of a point process on spatial covariates. *Statistics and Its Interface*
785 5 (2), 221–236.
- 786 Baddeley, A., Rubak, E., Turner, R., 2015. *Spatial Point Patterns: Methodology and*
787 *Applications* with R. Chapman and Hall/CRC, London.
- 788 Bar-Yosef, O., Tchernov, E., 1972. On the palaeo-ecological history of the site of Ubei-
789 diya. Vol. 35. Israel Academy of Sciences and Humanities, Jerusalem.
- 790 Benito-Calvo, A., de la Torre, I., 2011. Analysis of orientation patterns in Olduvai
791 Bed I assemblages using GIS techniques: Implications for site formation processes.
792 *Journal of Human Evolution* 61 (1), 50 – 60.
- 793 Benito-Calvo, A., Martínez-Moreno, J., Mora, R., Roy, M., Roda, X., 2011. Tram-
794 pling experiments at cova gran de santa linya, pre-pyrenees, spain: their relevance
795 for archaeological fabrics of the upper-middle paleolithic assemblages. *Journal of*
796 *Archaeological Science* 38 (12), 3652 – 3661.
- 797 Benito-Calvo, A., Martínez-Moreno, J., Pardo, J. F. J., de la Torre, I., Torcal, R. M.,
798 2009. Sedimentological and archaeological fabrics in Palaeolithic levels of the
799 South-Eastern Pyrenees: Cova Gran and Roca dels Bous Sites (Lleida, Spain). *Jour-*
800 *nal of Archaeological Science* 36 (11), 2566 – 2577.
- 801 Benn, D., 1994. Fabric shape and the interpretation of sedimentary fabric data. *Journal*
802 *of Sedimentary Research* 64 (4a), 910–915.
- 803 Berman, M., 1986. Testing for spatial association between a point process and another
804 stochastic process. *Applied Statistics* 35, 54–62.

- 805 Bernatchez, J. A., 2010. Taphonomic implications of orientation of plotted finds from
806 Pinnacle Point 13B (Mossel Bay, Western Cape Province, South Africa). *Journal of*
807 *Human Evolution* 59 (3–4), 274 – 288.
- 808 Bertran, P., Hetù, B., Texier, J.-P., Steijn, H. V., 1997. Fabric characteristics of subaerial
809 slope deposits. *Sedimentology* 44 (1), 1 – 16.
- 810 Bertran, P., Lenoble, A., Todisco, D., Desrosiers, P. M., Sørensen, M., 2012. Particle
811 size distribution of lithic assemblages and taphonomy of Palaeolithic sites. *Journal*
812 *of Archaeological Science* 39 (10), 3148 – 3166.
- 813 Bertran, P., Texier, J.-P., 1995. Fabric Analysis: Application to Paleolithic Sites. *Jour-*
814 *nal of Archaeological Science* 22 (4), 521 – 535.
- 815 Boschian, G., Saccà, D., 2010. Ambiguities in human and elephant interactions? sto-
816 ries of bones, sand and water from castel di guido (italy). *Quaternary International*
817 214 (1–2), 3 – 16, geoarchaeology and Taphonomy.
- 818 Carrer, F., 2015. Interpreting intra-site spatial patterns in seasonal contexts: an ethnoar-
819 chaeological case study from the western alps. *Journal of Archaeological Method*
820 *and Theory*, 1–25.
- 821 Clark, A. E., 2016. Time and space in the middle paleolithic: Spatial structure and
822 occupation dynamics of seven open-air sites. *Evolutionary Anthropology: Issues,*
823 *News, and Reviews* 25 (3), 153–163.
- 824 Cobo-Sánchez, L., Aramendi, J., Domínguez-Rodrigo, M., 2014. Orientation patterns
825 of wildebeest bones on the lake masek floodplain (serengeti, tanzania) and their
826 relevance to interpret anisotropy in the olduvai lacustrine floodplain. *Quaternary In-*
827 *ternational* 322–323 (0), 277 – 284, the Evolution of Hominin Behavior during the
828 Oldowan-Acheulian Transition: Recent Evidence from Olduvai Gorge and Peninj
829 (Tanzania).
- 830 Diggle, P., 1985. A kernel method for smoothing point process data. *Applied Statistics*
831 (*Journal of the Royal Statistical Society, Series C*) 34, 138–147.

- 832 Domínguez-Rodrigo, M., Bunn, H., Mabulla, A., Baquedano, E., Uribelarrea, D.,
833 Pérez-González, A., Gidna, A., Yravedra, J., Diez-Martin, F., Egeland, C., Barba,
834 R., Arriaza, M., Organista, E., Ansón, M., 2014a. On meat eating and human evolu-
835 tion: A taphonomic analysis of BK4b (Upper Bed II, Olduvai Gorge, Tanzania), and
836 its bearing on hominin megafaunal consumption. *Quaternary International* 322–323,
837 129–152.
- 838 Domínguez-Rodrigo, M., Bunn, H., Pickering, T., Mabulla, A., Musiba, C., Baque-
839 dano, E., Ashley, G., Diez-Martin, F., Santonja, M., Uribelarrea, D., Barba, R.,
840 Yravedra, J., Barboni, D., Arriaza, C., Gidna, A., 2012. Autochthony and orientation
841 patterns in Olduvai Bed I: a re-examination of the status of post-depositional biasing
842 of archaeological assemblages from FLK North (FLKN). *Journal of Archaeological
843 Science* 39 (7), 2116 – 2127.
- 844 Domínguez-Rodrigo, M., Cobo-Sánchez, L., Yravedra, J., Uribelarrea, D., Arriaza, C.,
845 Organista, E., Baquedano, E., 2017. Fluvial spatial taphonomy: a new method for the
846 study of post-depositional processes. *Archaeological and Anthropological Sciences*,
847 1–21.
- 848 Domínguez-Rodrigo, M., Diez-Martín, F., Yravedra, J., Barba, R., Mabulla, A., Baque-
849 dano, E., Uribelarrea, D., Sánchez, P., Eren, M. I., 2014b. Study of the SHK Main
850 Site faunal assemblage, Olduvai Gorge, Tanzania: Implications for Bed II taphon-
851 omy, paleoecology, and hominin utilization of megafauna. *Quaternary International*
852 322–323, 153–166.
- 853 Domínguez-Rodrigo, M., García-Pérez, A., 07 2013. Testing the accuracy of different
854 a-axis types for measuring the orientation of bones in the archaeological and pale-
855 ontological record. *PLoS ONE* 8 (7), e68955.
- 856 Domínguez-Rodrigo, M., Uribelarrea, D., Santonja, M., Bunn, H., García-Pérez, A.,
857 Pérez-González, A., Panera, J., Rubio-Jara, S., Mabulla, A., Baquedano, E., Yrave-
858 dra, J., Diez-Martín, F., 2014c. Autochthonous anisotropy of archaeological mate-
859 rials by the action of water: experimental and archaeological reassessment of the

- 860 orientation patterns at the olduvai sites. *Journal of Archaeological Science* 41 (0),
861 44 – 68.
- 862 Eren, M. I., Durant, A., Neudorf, C., Haslam, M., Shipton, C., Bora, J., Korisettar,
863 R., Petraglia, M., 2010. Experimental examination of animal trampling effects on
864 artifact movement in dry and water saturated substrates: a test case from south india.
865 *Journal of Archaeological Science* 37 (12), 3010 – 3021.
- 866 García-Moreno, A., Smith, G. M., Kindler, L., Pop, E., Roebroeks, W., Gaudzinski-
867 Windheuser, S., Klinkenberg, V., 2016. Evaluating the incidence of hydrological pro-
868 cesses during site formation through orientation analysis. a case study of the middle
869 palaeolithic lakeland site of neumark-nord 2 (germany). *Journal of Archaeological*
870 *Science: Reports* 6, 82 – 93.
- 871 Gifford-Gonzalez, D., Damrosch, D., Damrosch, D., Pryor, J., Thunen, R., 1985. The
872 third dimension in site structure: An experiment in trampling and vertical dispersal.
873 *American Antiquity* 50 (4), 803–818.
- 874 Giusti, D., Arzarello, M., 2016. The need for a taphonomic perspective in spatial anal-
875 ysis: Formation processes at the early pleistocene site of pirro nord (p13), apricena,
876 italy. *Journal of Archaeological Science: Reports* 8, 235 – 249.
- 877 Harvati, K., Panagopoulou, E., Tourloukis, V., Thompson, N., Karkanas, P., Athanas-
878 siou, A., Konidaris, G., Tsartsidou, G., Giusti, D., 2016. New middle pleistocene
879 elephant butchering site from greece. In: Paleoanthropology Society Meeting. At-
880 lanta, Georgia, pp. A14–A15.
- 881 Hivernel, F., Hodder, I., 1984. Analysis of artifact distribution at ngenyem (kenya):
882 depositional and postdepositional effects. In: Hietala, H., Larson, P. (Eds.), *Intrasite*
883 *Spatial Analysis in Archaeology*. Cambridge University Press, Ch. 7, pp. 97–115.
- 884 Hodder, I., Orton, C., 1976. *Spatial Analysis in Archaeology*. New Studies in Archae-
885 ology. Cambridge University Press, Cambridge.
- 886 Isaac, G. L., 1967. Towards the interpretation of occupation debris: Some experiments
887 and observations. *Kroeber Anthropological Society Papers* 37 (37), 31–57.

- 888 Jammalamadaka, S., Sengupta, A., Sengupta, A., 2001. Topics in Circular Statistics.
889 Series on multivariate analysis. World Scientific.
- 890 Lenoble, A., 2005. Ruissellement et formation des sites préhistoriques. Référentiel ac-
891 tualiste et exemple d'application au fossile. Vol. 1363 of International Series. British
892 Archaeological Report, Oxford.
- 893 Lenoble, A., Bertran, P., 2004. Fabric of Palaeolithic levels: methods and implications
894 for site formation processes. Journal of Archaeological Science 31 (4), 457 – 469.
- 895 Lenoble, A., Bertran, P., Lacrampe, F., 2008. Solifluction-induced modifications
896 of archaeological levels: simulation based on experimental data from a modern
897 periglacial slope and application to French Palaeolithic sites. Journal of Archaeo-
898 logical Science 35 (1), 99 – 110.
- 899 López-Ortega, E., Bargalló, A., de Lombera-Hermida, A., Mosquera, M., Ollé, A.,
900 Rodríguez-Álvarez, X. P., 2015. Quartz and quartzite refits at gran dolina (sierra
901 de atapuerca, burgos): Connecting lithic artefacts in the middle pleistocene unit of
902 td10.1. Quaternary International, –.
- 903 López-Ortega, E., Rodríguez, X. P., Vaquero, M., 2011. Lithic refitting and movement
904 connections: the NW area of level TD10-1 at the Gran Dolina site (Sierra de Ata-
905 puerca, Burgos, Spain). Journal of Archaeological Science 38 (11), 3112 – 3121.
- 906 Marwick, B., 2017. Computational reproducibility in archaeological research: Ba-
907 sical principles and a case study of their implementation. Journal of Archaeological
908 Method and Theory 24 (2), 424–450.
- 909 McPherron, S. J., 2005. Artifact orientations and site formation processes from total
910 station proveniences. Journal of Archaeological Science 32 (7), 1003 – 1014.
- 911 Morin, E., Tsanova, T., Sirakov, N., Rendu, W., Mallye, J.-B., Lèveque, F., 2005. Bone
912 refits in stratified deposits: testing the chronological grain at saint-cesaire. Journal
913 of Archaeological Science 32, 1083–1098.

- 914 Morton, A. G. T., 2004. Archaeological Site Formation: Understanding Lake Margin
915 Contexts. No. 1211 in BAR International Series. Archaeopress, Oxford.
- 916 Nickel, B., Riegel, W., Schonherr, T., Velitzelos, E., 1996. Environments of coal forma-
917 tion in the pleistocene lignite at megalopolis, peloponnesus (greece) - reconstruction
918 from palynological and petrological investigations. N. Jb. Geol. Palaont. A. 200,
919 201–220.
- 920 Nielsen, A. E., 1991. Trampling the archaeological record: an experimental study.
921 Americal Antiquity 56 (3), 483–503.
- 922 Ohser, J., 1983. On estimators for the reduced second moment measure of point pro-
923 cesses. Mathematische Operationsforschung und Statistik, series Statistics 14, 63–
924 71.
- 925 Organista, E., Domínguez-Rodrigo, M., Yravedra, J., Uribelarrea, D., Arriaza, M. C.,
926 Ortega, M. C., Mabulla, A., Gidna, A., Baquedano, E., 2017. Biotic and abiotic pro-
927 cesses affecting the formation of {BK} level 4c (bed ii, olduvai gorge) and their bear-
928 ing on hominin behavior at the site. Palaeogeography, Palaeoclimatology, Palaeo-
929 cology, –.
- 930 Orton, C., 1982. Stochastic process and archaeological mechanism in spatial analysis.
931 Journal of Archaeological Science 9 (1), 1 – 23.
- 932 Panagopoulou, E., Tourloukis, V., Thompson, N., Athanassiou, A., Tsartsidou, G.,
933 Konidaris, G., Giusti, D., Karkanas, P., Harvati, K., 2015. Marathousa 1: a new mid-
934 dle pleistocene archaeological site from greece. Antiquity Project Gallery 89 (343).
- 935 Petraglia, M. D., Nash, D. T., 1987. The impact of fluvial processes on experimen-
936 tal sites. In: Nash, D. T., Petraglia, M. D. (Eds.), Natural formation processes and
937 the archaeological record. Vol. 352 of International Series. British Archaeological
938 Reports, Oxford, pp. 108–130.
- 939 Petraglia, M. D., Potts, R., 1994. Water flow and the formation of early pleistocene
940 artifact sites in olduvai gorge, tanzania. Journal of Anthropological Archaeology
941 13 (3), 228 – 254.

- 942 Pierson, T. C., 2005. Distinguishing between debris flows and floods from field evi-
943 dence in small watersheds. Usgs numbered series, U.S. Geological Survey.
- 944 R Core Team, 2016. R: A Language and Environment for Statistical Computing. R
945 Foundation for Statistical Computing, Vienna, Austria.
- 946 Rick, J. W., 1976. Downslope movement and archaeological intrasite spatial analysis.
947 American Antiquity 41 (2), 133–144.
- 948 Ripley, B., 1977. Modelling spatial patterns. Journal of the Royal Statistical Society,
949 series B 39, 172–212.
- 950 Ripley, B., 1988. Statistical inference for spatial processes. Cambridge University
951 Press.
- 952 Ripley, B. D., 1976. The second-order analysis of stationary point processes. Journal
953 of Applied Probability 13 (2), 255–266.
- 954 Ripley, B. D., 1981. Spatial Statistics. John Wiley and Sons, New York.
- 955 Schick, K. D., 1984. Processes of paleolithic site formation: an experimental study.
956 Ph.D. thesis, University of California, Berkeley.
- 957 Schick, K. D., 1986. Stone Age sites in the making: experiments in the formation
958 and transformation of archaeological occurrences. Vol. 319 of International Series.
959 British Archaeological Reports, Oxford.
- 960 Schick, K. D., 1987. Modeling the formation of early stone age artifact concentrations.
961 Journal of Human Evolution 16, 789–807.
- 962 Schiffer, M. B., 1972. Archaeological context and systemic context. American Antiq-
963 uity 37 (2), 156–165.
- 964 Schiffer, M. B., 1983. Toward the identification of formation processes. American An-
965 tiquity 48 (4), 675–706.
- 966 Schiffer, M. B., 1987. Formation processes of the archaeological record. University of
967 New Mexico Press, Albuquerque.

- 968 Shackley, M. L., 1978. The behaviour of artefacts as sedimentary particles in a fluvial
969 environment. *Archaeometry* 20 (1), 55–61.
- 970 Sisk, M. L., Shea, J. J., 2008. Intrasite spatial variation of the omo kibish middle
971 stone age assemblages: Artifact refitting and distribution patterns. *Journal of Human
972 Evolution* 55 (3), 486 – 500, paleoanthropology of the Kibish Formation, Southern
973 Ethiopia.
- 974 Sánchez-Romero, L., Benito-Calvo, A., Pérez-González, A., Santonja, M., 12 2016.
975 Assessment of accumulation processes at the middle pleistocene site of ambrona
976 (soria, spain). density and orientation patterns in spatial datasets derived from exca-
977 vations conducted from the 1960s to the present. *PLOS ONE* 11 (12), 1–27.
- 978 Todd, L., Stanford, D., 1992. Application of conjoined bone data to site structural
979 studies. In: Hofman, J., Enloe, J. (Eds.), *Piecing Together the Past: Applications of
980 Refitting Studies in Archaeology*. Vol. 578 of International Series. BAR, Oxford, pp.
981 21–35.
- 982 van Vugt, N., de Bruijn, H., van kolfschoten, M., Langereis, C. G., 2000. Magneto-
983 and cyclostratigraphy and mammal-fauna's of the pleistocene lacustrine megalopolis
984 basin, peloponnesos, greece. *Geologica Ultrajectina* 189, 69–92.
- 985 Vaquero, M., Bargalló, A., Chacón, M. G., Romagnoli, F., Sañudo, P., 2015. Lithic
986 recycling in a middle paleolithic expedient context: Evidence from the abric romaní
987 (capellades, spain). *Quaternary International* 361, 212 – 228, the Origins of Recy-
988 cling: A Paleolithic Perspective.
- 989 Vaquero, M., Chacón, M. G., García-Antón, M. D., de Soler, B. G., Martínez, K.,
990 Cuartero, F., 2012. Time and space in the formation of lithic assemblages: The
991 example of Abric Romaní Level J. *Quaternary International* 247 (0), 162 – 181,
992 <ce:title>The Neanderthal Home: spatial and social behaviours</ce:title>.
- 993 Villa, P., 1982. Conjoinable pieces and site formation processes. *American Antiquity*
994 47 (2), 276–290.

- 995 Villa, P., 1990. Torralba and aridos: elephant exploitation in middle pleistocene spain.
- 996 Journal of Human Evolution 19 (3), 299 – 309.
- 997 Villa, P., Courtin, J., 1983. The interpretation of stratified sites: A view from under-
- 998 ground. Journal of Archaeological Science 10 (3), 267–281.
- 999 Voorhies, M., 1966. Taphonomy and population dynamics of an early pliocene verte-
- 1000 brate fauna, knox county, nebraska. Ph.D. thesis, University of Wyoming.
- 1001 Wood, R. W., Johnson, D. L., 1978. A survey of disturbance processes in archaeologi-
- 1002 cal site formation. In: Schiffer, M. B. (Ed.), Advances in archaeological method and
- 1003 theory. Vol. 1. Academic Press, Ch. 9, pp. 315–381.
- 1004 Woodcock, N., Naylor, M., 1983. Randomness testing in three-dimensional orientation
- 1005 data. Journal of Structural Geology 5 (5), 539 – 548.